Front. Struct. Civ. Eng. 2019, 13(5): 1082–1094
https://doi.org/10.1007/s11709-019-0537-3

RESEARCH ARTICLE

Variational mode decomposition based modal parameter identification in civil engineering

Mingjie ZHANG, Fuyou XU*

School of Civil Engineering, Dalian University of Technology, Dalian 116024, China
**Corresponding author. E-mail: fuyouxu@hotmail.com*

ABSTRACT An out-put only modal parameter identification method based on variational mode decomposition (VMD) is developed for civil structure identifications. The recently developed VMD technique is utilized to decompose the free decay response (FDR) of a structure into to modal responses. A novel procedure is developed to calculate the instantaneous modal frequencies and instantaneous modal damping ratios. The proposed identification method can straightforwardly extract the mode shape vectors using the modal responses extracted from the FDRs at all available sensors on the structure. A series of numerical and experimental case studies are conducted to demonstrate the efficiency and highlight the superiority of the proposed method in modal parameter identification using both free vibration and ambient vibration data. The results of the present method are compared with those of the empirical mode decomposition-based method, and the superiorities of the present method are verified. The proposed method is proved to be efficient and accurate in modal parameter identification for both linear and nonlinear civil structures, including structures with closely spaced modes, sudden modal parameter variation, and amplitude-dependent modal parameters, etc.

KEYWORDS modal parameter identification, variational mode decomposition, civil structure, nonlinear system, closely spaced modes

1 Introduction

Modal parameters (modal frequencies, modal damping ratios, and mode shape vectors) are key parameters of civil structures. The identification of modal parameters belongs to the inverse problems [1,2] (which also include the control problem and optimization problem, etc.), and is an important topic in the engineering domain. Modal parameter identification has found applications in design assumption validation [3], non-destructive damage detection [4], health monitoring [5], dynamic response analysis [6], and vibration control [7], etc. Modal parameters are generally identified through the acceleration (or displacement) responses recorded during dynamic tests, which include three basic types, i.e., force vibration test, free vibration test, and ambient vibration test (measuring the vibration response under ambient excitation, e.g., wind, traffic, etc.). Generally, it is hard to quantify the external input (excitation force) on a real structure, and the external input may disturb the normal operation of the structure. Therefore, the ambient vibration test-based methods have been extensively studied, and are often referred to as output-only methods. Some free vibration test-based methods can also be classified as output-only methods since the input is not necessary to be measured, and the modal parameters can be extracted from the free decay responses (FDRs) [8,9].

Classic output-only system identification methods can be classified into frequency domain methods and time domain methods. The frequency domain methods include the peak-picking method [10], the frequency domain decomposition method [11], the enhanced frequency domain decomposition method [12], and the frequency-spatial domain method [13], etc. These methods are quite straightforward to implement, while their abilities are very limited for many types of systems, especially for systems with high damping ratios and closely spaced modes. The time domain methods include the random decrement technique (RDT) [14], the eigensystem realization algorithm [15], the autoregressive moving average method [16], the stochastic subspace identification method [17], and the method based on proper orthogonal decomposition

Article history: Received Jun 24, 2018; Accepted Sep 16, 2018

[18], etc. The time domain methods avoid some limitations (e.g., low frequency resolution) of the Fourier based frequency domain methods, and make online system identification of an in-operation structure possible. However, both the classic time domain methods and frequency domain methods are inefficient to identify the nonlinear and nonstationary features in civil structures, which may be induced by structural damage, material nonlinearity, and geometric nonlinearity, etc. Some sensitivity analysis methods have also been developed to investigate the uncertainties in the modal parameters of complicated structures and to deal with the effects of noise [19–21].

Modal parameter identification methods based on time-frequency analysis have received increasing attentions in recent years since they can provide both time and frequency information of a signal simultaneously and are suitable to deal with nonlinear and nonstationary signals. The wavelet transform(WT)-based methods [22] and methods based on the empirical mode decomposition (EMD) with Hilbert transform (HT) [23–29] are among the most popular ones. The multi-resolution and time-frequency analysis capabilities of the WT have promoted its successful applications in system identifications of many types of structures. However, due to its non-adaptive property, a major difficulty of the WT-based methods is to select an appropriate mother wavelet for any analysis. The EMD is an adaptive signal processing technique, and its combination with the HT provides another powerful time-frequency analysis tool, which is often referred to as the Hilbert-Huang transform (HHT). EMD decomposes a complicated multi-component signal into the summations of a finite number of mono-component signals referred to as intrinsic mode functions (IMFs), and the HT is then applied to the IMFs to calculate their instantaneous amplitudes and instantaneous frequencies. A time-frequency representation of the multi-component signal can be obtained and the modal parameters can be subsequently extracted. Yang et al. [25,26] proposed a modal identification method for linear systems using free vibration data based on the HHT method, and showed that the HHT-based method can serve as an effective tool for linear system identification. Chen et al. [27] combined the HHT and RDT to identify the modal parameters of Tsing Ma suspension bridge using the ambient vibration data caused by Typhoon Victor. Pines and Salvino [28] identified the modal parameters of a 3-story building model with a HHT-based method, and detected the damage with the phase information. He et al. [29] presented an EMD-based RDT method, and the method was verified through the modal parameter identification of an existing railway bridge. Shi and Law [30] showed the ability of the HHT-based method in identifying typical time-varying systems. Moreover, some improved versions of HHT [31,32] have been developed and applied to structure identifications, by which the performances of the HHT-based methods can be improved.

Despite the wide application of HHT, it has some limitations associated with the EMD process: 1) the first IMF generally covers a wide frequency range and may not be a mono-component signal [32]; 2) its performance varies with the frequency ratios and amplitude ratios of the inherent modes in a signal, so that closely spaced modes and low-energy modes cannot be reliably separated [33]; 3) some low-energy pseudo-components may be generated in the low-frequency region [31]; 4) it is sensitive to noises and sampling frequency of the recorded signal [34]. To overcome these shortcomings, the variational mode decomposition (VMD) [34] is recently proposed as another adaptive signal decomposition technique. VMD decomposes a complicated multi-component signal into several mono-component modes which collectively reproduce the original signal. This method is non-recursive and extracts the modes concurrently. The superiority of VMD relative to EMD in processing certain types of signals has been demonstrated in seismic signal analysis [35], power signal analysis [36], speech signal analysis [37], and fault diagnosis [38]. Recently, Bagheri et al. [9] proposed a structural system identification method using free vibration test data based on VMD. However, it is only applicable for linear systems. The efficiency of the VMD-based method to identify nonlinear and nonstationary features with both free vibration and ambient vibration test data is worth to be investigated.

In the present work, an out-put only modal parameter identification method based on VMD is developed for civil structure identifications. In the proposed method, the FDR (recorded in free vibration test or reconstructed from ambient vibration response) of a structure is first decomposed into modal responses using VMD. The instantaneous frequencies of the modal responses are calculated with the empirical envelope (EE) method [39], and the instantaneous modal damping ratios are calculated using a newly developed procedure. All instantaneous modal frequencies and instantaneous modal damping ratios can be identified using a single acceleration history measurement at a suitable location, and the calculated instantaneous modal frequencies and instantaneous modal damping ratios can capture any transient modal parameter variations. Mode shape vectors can also be identified if multiple sensor locations are available on the structure. To verify the efficiency and highlight the superiority of the proposed method, a series of numerical and experimental examples are carried out. The examples demonstrate the efficiency and superiority of the proposed method in modal parameter identification with both free vibration and ambient vibration data.

2 Presentation of proposed method

The proposed VMD-based modal parameter identification method includes three main steps: 1) the modal responses

are extracted from the FDR recorded in a free vibration test or reconstructed from ambient vibration response (e.g., by RDT [14]); 2) the instantaneous modal frequency and instantaneous modal damping ratio of each mode are extracted from the corresponding modal response; 3) the mode shape vectors are identified by processing the modal responses extracted from the FDRs at all available sensors on the structure. Details of each step are illustrated in the following part of this section.

2.1 Extracting modal responses: VMD

VMD is used to decompose a FDR (denoted as $s(t)$) into a finite number of mono-component sub-signals (modes), i.e.,

$$s(t) = \sum_{k=1}^{K} v_k(t), \tag{1}$$

where $\{v_k(t)\} = \{v_1(t), ..., v_K(t)\}$ denotes the set of all sub-signals, and each sub-signal is compact around a center frequency ($\{f_k\} = \{f_1,..., f_K\}$) and represents a distinct modal response of the structure; K is the decomposition level which needs to be specified by the operator.

The decomposition is realized by solving the following constrained variational problem

$$\min_{\{v_k\},\ \{f_k\}} \left\{ \sum_{k=1}^{K} \left\| \partial_t \left[\left(\delta(t) + \frac{j}{\pi t} \right) * v_k(t) \right] \mathrm{e}^{-j2\pi f_k t} \right\|_2^2 \right\}, \tag{2}$$

where ∂_t represents the derivative with respect to time; $\delta(t)$ is the Dirac distribution; $j = \sqrt{-1}$; '$*$' denotes the convolution operation; '$\| \ \|_2$' denotes the L2 norm.

A quadratic penalty term and Lagrangian multiplier (denoted as λ) are used to render the problem unconstrained, resulting in an augmented Lagrangian (denoted as L) given by

$$\begin{aligned} &L(\{v_k(t)\},\ \{f_k\},\ \lambda(t)) \\ &= \alpha \sum_{k=1}^{K} \left\| \partial_t \left[\left(\delta(t) + \frac{j}{\pi t} \right) * v_k(t) \right] \mathrm{e}^{-j2\pi f_k t} \right\|_2^2 \\ &+ \left\| s(t) - \sum_{k=1}^{K} v_k(t) \right\|_2^2 + \left\langle \lambda(t),\ s(t) - \sum_{k=1}^{K} v_k(t) \right\rangle, \end{aligned} \tag{3}$$

where α represents the balancing parameter of the data fidelity constraint; '$\langle\ \rangle$' denotes the inner product of two vectors.

The solution to the original minimization problem in Eq. (2) is now found as the saddle point of L, and can be solved with a sequence of iterative sub-optimizations named alternate direction method of multipliers (ADMM) [40]. The ADMM searches v_k and f_k in the frequency domain with an iterative procedure given by

$$\hat{v}_k^{n+1}(f) = \frac{\hat{s}(f) - \sum_{i \neq k} \hat{v}_i^n(f) + \hat{\lambda}^n(f)/2}{1 + 2\alpha(2\pi f - 2\pi f_k^n)^2}, \tag{4a}$$

$$f_k^{n+1} = \frac{\int_0^\infty 2\pi f |\hat{v}_k^n(f)|^2 \mathrm{d}f}{\int_0^\infty |\hat{v}_k^n(f)|^2 \mathrm{d}f}, \tag{4b}$$

where superscript n denotes the nth iterative step; '$\wedge$' denotes the Fourier transform of a signal. The iterative process terminates while $\dfrac{\sum \left\| v_k^{n+1} - v_k^n \right\|_2^2}{\sum \left\| v_k^n \right\|_2^2} < \varepsilon$, where ε is pre-specified small number.

The final solution for $v_k(t)$ can be obtained as the real part of the inverse Fourier transform of $\hat{v}_k(f)$, i.e.,

$$v_k(t) = R\{ifft(\hat{v}_k(f))\}. \tag{5}$$

Detailed introductions of VMD and a Matlab code for reference implementation can be found in Ref. [34]. It should be stated that the decomposition results of VMD is closely related to the selection of the value of K. Some typical signs of over-decomposition ($K >$ actual mode number) and under-decomposition ($K <$ actual mode number) can be found in Ref. [34]. Besides, some algorithms have been developed to select the value of K [38,41]. In the present work, K is simply selected according to the number of dominant bands in the Fourier spectra. Although sometimes this method may fail to select the right value of K due to the limitation of frequency resolution of the Fourier transform, the signs in Ref. [34] can be used to evaluate over-decomposition or under-decomposition in such conditions.

For a system with constant modal frequencies, $\{f_k\} = \{f_1,..., f_K\}$ represent the damped modal frequencies of the structure since the FDRs used for structural identification contain the contributions of structural damping. The deviation between a damped modal frequency and the un-damped value increases with increasing the damping ratio [42], while the deviation is almost negligible (e.g., the relative error is around 0.5% for a damping ratio equals 0.1). For a system with time-varying modal frequencies, $\{f_k\} = \{f_1,..., f_K\}$ just represent the weighted means of the damped time-varying modal frequencies. To capture the possible nonlinear and/or nonstationary features of the modal responses, the instantaneous modal frequencies and instantaneous modal damping ratios can be calculated, which will be illustrated in the following part.

2.2 Identification of instantaneous modal frequency and instantaneous modal damping ratio

Each modal response is a mono-component signal with amplitude-modulation (AM) and frequency-modulation (FM), and can be expressed as

$$v(t) = q(t)\cos[\varphi(t)] = q(t)\cos\left[\int_0^t 2\pi f(\tau)\mathrm{d}\tau + \theta\right], \quad (6)$$

where $q(t)$ is the AM part (instantaneous amplitude); $\cos[\varphi(t)]$ is the FM part; $\varphi(t)$ is the instantaneous phase; $f(t)$ is the instantaneous frequency; θ is the initial phase.

$q(t)$ and $f(t)$ have been traditionally calculated using the HT. However, the HT may result in remarkable fluctuations or even negative values in the calculated $f(t)$ at some time instants due to the limitations of the Bedrosian theorem [43] and Nuttall theorem [44]. Recently, Huang et al. [45] introduced a normalized HT (NHT) method in which a mono-component signal is first decomposed into its AM and FM parts through an empirical AM-FM decomposition. HT is then applied to the FM part with constant amplitude, and thus the limitation of the Bedrosian theorem can be removed. Zheng et al. [39] further proposed an EE method on the basis of the AM-FM decomposition, which has been proved to perform better in calculating $f(t)$. Therefore, in this study, the EE method is used to calculate $q(t)$ and $f(t)$ of a mono-component signal. The process of the EE method is briefly illustrated in the Appendix.

Once $q(t)$ is obtained, the instantaneous logarithmic decrement $\delta(t)$ of $v(t)$ can be calculated as

$$\delta(t_m) = \ln\frac{q(t_m)}{q(t_{m-1})} = \frac{2\pi\xi(t_m)}{\sqrt{1-\xi^2(t_m)}}, \quad (7)$$

where m denotes the mth discrete sampling point; $\xi(t)$ is the instantaneous damping ratio of $v(t)$.

For case of low $\xi(t)$, it can be approximated as

$$\xi(t) = \frac{\ln[q(t_m)/q(t_{m-1})]}{2\pi}. \quad (8)$$

The error induced by Eq. (8) increases with increasing $\xi(t)$ [42], and it can be calculated that the relative error is lower than 0.5% for $\xi(t) < 0.1$.

The instantaneous modal frequencies and instantaneous modal damping ratios of a linear system should be almost constant, and variations in the instantaneous modal frequencies and instantaneous modal damping ratios can serve as simple indications of the existence of nonlinearities. A great number of laboratory and full-scale experiments show that the modal frequencies and modal damping ratios of many types of civil structures may be dependent on the vibration amplitudes [6,45,46]. Therefore, it is generally reasonable to transform $f(t)$ and $\xi(t)$ into the amplitude-dependent frequency and amplitude-dependent damping ratio, respectively, i.e.,

$$[q(t), f(t)] \xrightarrow{\text{polynomial fitting}} f(q), \quad (9a)$$

$$[q(t), \xi(t)] \xrightarrow{\text{polynomial fitting}} \xi(q). \quad (9b)$$

2.3 Identification of mode shapes

The mode shape vector for a specific mode can be straightforwardly indentified using the modal responses extracted from the FDRs at all available sensors. Assuming that there are totally n sensors available on a structure, the modal responses of the kth mode extracted from the FDRs at all n sensors are denoted as $v_k^1(t), v_k^2(t), \ldots, v_k^n(t)$, respectively. The instantaneous damping ratios of $v_k^i(t)$ (i = 1–n) all reflect the modal damping ratio of the k^{th} mode, so that the following relationship can be deduced from Eq. (8)

$$\frac{q_k^j(t_m)}{q_k^i(t_m)} = \frac{q_k^j(t_{m-1})}{q_k^i(t_{m-1})}, \quad (10)$$

where $q_k^i(t)$ and $q_k^j(t)$ are the instantaneous amplitudes of $v_k^i(t)$ and $v_k^j(t)$, respectively.

Equation (10) indicates that $q_k^j(t)/q_k^i(t)$ is constant theoretically. However, the calculated $q_k^j(t)/q_k^i(t)$ may exhibit slightly fluctuations due the noises, discrete sampling of the recorded signal, and cubic spline fitting in the EE method. Practically, the mean values of $q_k^j(t)/q_k^i(t)$ can be calculated to minimize the error, i.e.,

$$r_k^{ij} = \text{mean}[q_k^j(t)/q_k^i(t)]. \quad (11)$$

The normalized mode shape vector of the kth mode can be obtained as

$$\Phi_k = [1, r_k^{12}, \ldots, r_k^{1n}]^{\mathrm{T}}. \quad (12)$$

The mode shape vectors of all modes can be obtained by repeating the procedure in Eqs. (11) and (12).

3 Modal parameter identification from free vibration response

VMD overcomes some shortcomings of EMD while keeps the abilities of decomposing multi-component signal and detecting transient amplitude and/or frequency variation. Therefore, VMD is more suitable for the time-frequency analyses of certain types of nonlinear and nonstationary signals, and the proposed modal parameter identification method may perform better than the EMD or wavelet-based methods in dealing with some certain types of structures. In this section, three examples (with free vibration responses) are conducted to demonstrate the efficiency and superiority of the proposed method.

3.1 3-DOF system with closely space modes

The first example is a 3-DOF numerical system with very closely spaced modes. The motion equation of the numerical system can be expressed as

$$\boldsymbol{m}\ddot{\mathrm{x}} + \boldsymbol{c}\dot{\mathrm{x}} + \boldsymbol{k}\mathrm{x} = 0, \tag{13}$$

where $\boldsymbol{m}$, $\boldsymbol{k}$, and $\boldsymbol{c}$ are the mass, stiffness, and damping matrices, respectively; $\boldsymbol{x}$, $\dot{\boldsymbol{x}}$, $\ddot{\boldsymbol{x}}$ are the displacement, velocity, and acceleration vectors, respectively. $\boldsymbol{m}$, $\boldsymbol{k}$, and $\boldsymbol{c}$ are defined as

$$\boldsymbol{m} = m_0\boldsymbol{I}, \tag{14a}$$

$$\boldsymbol{k} = k_0\begin{bmatrix} 4 & -1 & 0 \\ -1 & 2 & -1 \\ 0 & -1 & 4 \end{bmatrix}, \tag{14b}$$

$$\boldsymbol{c} = [\boldsymbol{m}\boldsymbol{\Phi}\boldsymbol{M}^{-1}]\begin{bmatrix} 2\xi\omega_1 M_1 & 0 & 0 \\ 0 & 2\xi\omega_2 M_2 & 0 \\ 0 & 0 & 2\xi\omega_3 M_3 \end{bmatrix}[\boldsymbol{M}^{-1}\boldsymbol{\Phi}^{\mathrm{T}}\boldsymbol{m}], \tag{14c}$$

where m_0 = 1000 kg, k_0 = 10 kN/m, and ξ = 0.01; $\boldsymbol{I}$ is the unit matrix; $\boldsymbol{\Phi}$ is the mode shape matrix; $\omega_i = 2\pi f_i$ (i = 1 – 3) are the modal circular frequencies; $\boldsymbol{M}$ is the modal mass matrix, and M_i (i = 1 – 3) are the modal masses.

The theoretical natural frequencies of 3 modes are 0.567, 1.006, and 1.095 Hz, respectively, and the theoretical damping ratios of 3 modes are 0.01. The natural frequencies of the latter two modes are within 10% of each other, and can be considered as very closely spaced modes. The system is excited by a unit acceleration impulse (1 cm/s^2) at the third DOF, and the FDR at the third DOF and its amplitude spectra is shown in Fig. 1. Kijewski and Kareem [22] identified the modal parameters of the system with the same FDR using the Morlet wavelet-based analysis, and showed that the appropriate selection of the central frequency is of crucial importance to the identification accuracy.

To identify the modal parameters using the proposed method, the FDR in Fig. 1 is decomposed into 3 modes (by setting K = 3) using VMD as its amplitude spectra indicate that the signal has three dominate bands. The decomposition results are shown in Fig. 2, in which each mode (denoted as $v_1(t)$, $v_2(t)$, $v_3(t)$, respectively) represents a distinct modal response. Applying EMD (with the stopping criterion in Ref. [19]) to the FDR results in 8 IMFs (denoted as IMF$_i$ (i = 1 – 8)), as shown in Fig. 3. EMD successfully separates the first mode (f_1 = 0.567 Hz) while fails to separate the later two modes with closely spaced frequencies. Besides, 5 low-energy pseudo-components are generated in the EMD results, which might be misleading when dealing with a system without prior knowledge.

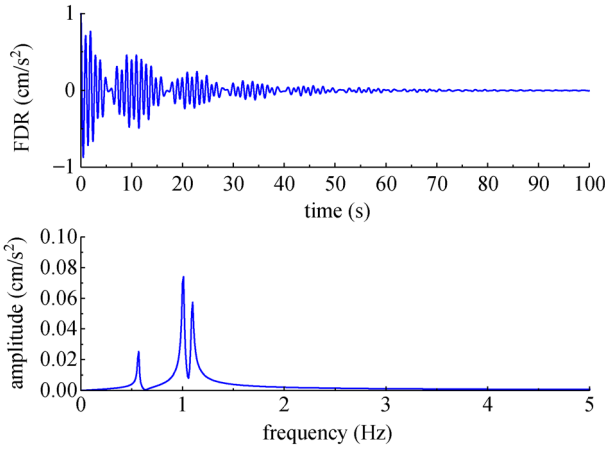

Fig. 1 FDR of a 3-DOF system and amplitude spectra

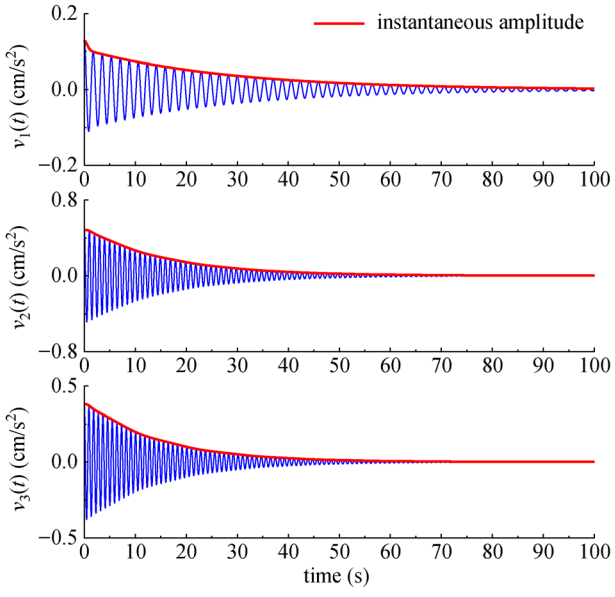

Fig. 2 Modal responses of a 3-DOF system and instantaneous amplitudes

The instantaneous amplitudes and instantaneous frequencies (denoted as $f_1(t)$, $f_2(t)$, $f_3(t)$, respectively) of the modal responses are calculated using the EE method, as shown in Figs. 2 and 4, respectively. The instantaneous amplitude agrees very well with the peaks of the corresponding modal response. $f_1(t)$, $f_2(t)$, $f_3(t)$ are very close to 0.567, 1.006, and 1.095 Hz, respectively. The results demonstrate that the system has constant modal frequencies as $f_1(t)$, $f_2(t)$, $f_3(t)$ almost do not vary with time. $f_1(t)$ calculated by the traditional HT is also shown in Fig. 4 for comparison. It can be seen that $f_1(t)$ obtained by the traditional HT agrees well with the theoretical result at the preliminary stage, and significantly deviates from the

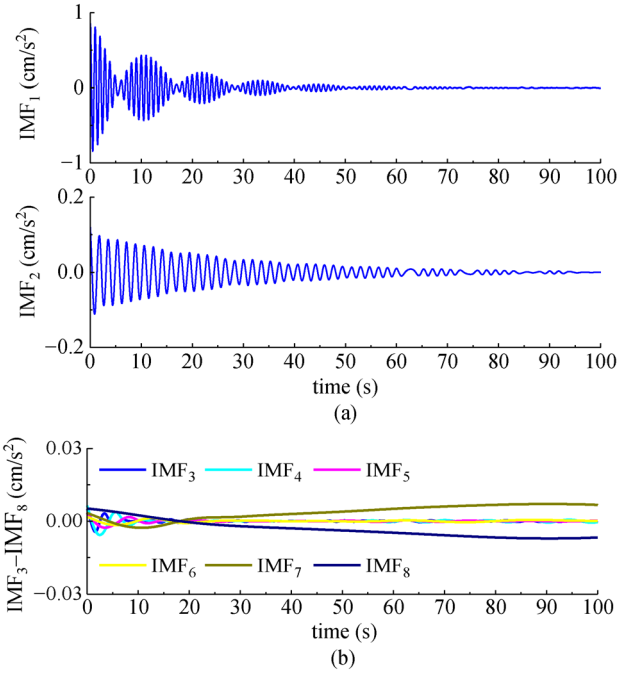

Fig. 3 EMD results for FDR of a 3-DOF system. (a) IMF_1 and IMF_2; (b) $IMF_3 \sim IMF_8$

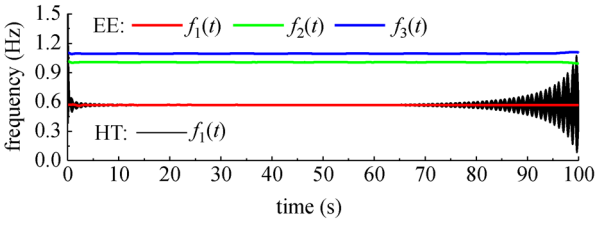

Fig. 4 Modal frequencies of a 3-DOF system

theoretical result at the later stage due to the end effect. Therefore, the advantage of the EE method is demonstrated obviously. The instantaneous modal damping ratios (denoted as $\xi_1(t)$, $\xi_2(t)$, $\xi_3(t)$, respectively) are calculated using Eq. (8), and the results are shown in Fig. 5. $\xi_1(t)$, $\xi_2(t)$, $\xi_3(t)$ are very close to 0.01, indicating the identification accuracy of the modal damping ratios. $\xi_1(t)$, $\xi_2(t)$, $\xi_3(t)$ exhibit slight fluctuations at the ends due to the end effect of the EE method. However, the end effects are quite weak compared with the results of the Morlet wavelet-based analysis in Ref. [22].

The instantaneous modal frequencies and instantaneous

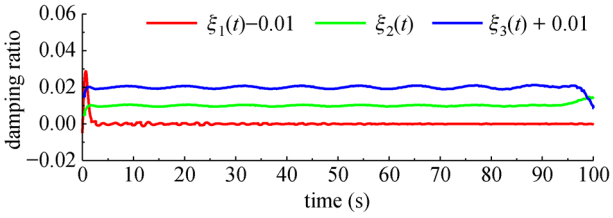

Fig. 5 Modal damping ratios of a 3-DOF system

modal damping ratios are extracted from the FDRs at all 3 DOFs separately, and the mean values of the instantaneous modal frequencies and instantaneous modal damping ratios are listed in Table 1. It can be seen that the mean values almost exactly reflect the theoretical values. The results for Mode 2 cannot be extracted from the FDR at the second DOF because the FDR does not contain the component of Mode 2 (the mode shape vector of Mode 2 is $[1.00\ 0.00\ -1.00]^{\mathrm{T}}$, as demonstrated later).

The accuracy of the proposed method is also investigated under different signal-to-noise ratios (SNRs). Gaussian white noises of different levels are added to the FDR in Fig. 1, and the modal parameters are extracted from the noisy signals by using the proposed method. The mean values of the instantaneous modal frequencies and instantaneous modal damping ratios extracted from the noisy signals of different SNRs are listed in Table 2. It can be seen that the identification error are negligible except for that of the modal damping ratio of Mode 1, mainly because the energy of the component of Mode 1 in the FDR is low so that extracted modal response is largely affected by noise. The preceding analysis demonstrates that the proposed method performs well in modal parameter identification from noisy signals.

The mode shape vectors can be identified from the modal responses at all 3 DOFs using the procedure in Section 2.3. As an example, the modal responses for Mode 1 at all 3 DOFs (denoted as $v_1^1(t)$,$v_1^2(t)$,$v_1^3(t)$, respectively) and their instantaneous amplitudes are shown in Fig. 6. The amplitude ratios between $v_1^2(t)$ and $v_1^1(t)$ (denoted as $r_1^{12}(t)$), and between $v_1^3(t)$ and $v_1^1(t)$ (denoted as $r_1^{13}(t)$) are shown in Fig. 7. It can be seen that $r_1^{12}(t)$ and $r_1^{13}(t)$ are almost constant. The normalized mode shape vector of Mode 1 can be obtained as $[1,\ r_1^{12},\ r_1^{13}]^{\mathrm{T}}$, where r_1^{12} and r_1^{13} are the mean values of $r_1^{12}(t)$ and $r_1^{13}(t)$, respectively. The identified mode shape vectors are listed in Table 3, in which the theoretical results are also shown for compar-

Table 1 Mean values of modal frequencies and modal damping ratios of a 3-DOF system

mode	mean[$f(t)$]			mean[$\xi(t)$]		
	1st DOF	2nd DOF	3rd DOF	1st DOF	2nd DOF	3rd DOF
1	0.567	0.567	0.568	0.010	0.010	0.010
2	1.006	unavailable	1.006	0.010	unavailable	0.010
3	1.095	1.094	1.095	0.010	0.010	0.010

Table 2 Mean values of modal frequencies and modal damping ratios of a 3-DOF system for different SNRs

SNR (dB)	mean[$f(t)$]			mean[$\xi(t)$]		
	Mode 1	Mode 2	Mode 3	Mode 1	Mode 2	Mode 3
40	0.567	1.006	1.095	0.010	0.010	0.010
30	0.567	1.006	1.095	0.011	0.010	0.010
20	0.570	1.009	1.097	0.012	0.010	0.010
10	0.572	1.010	1.099	0.012	0.011	0.011

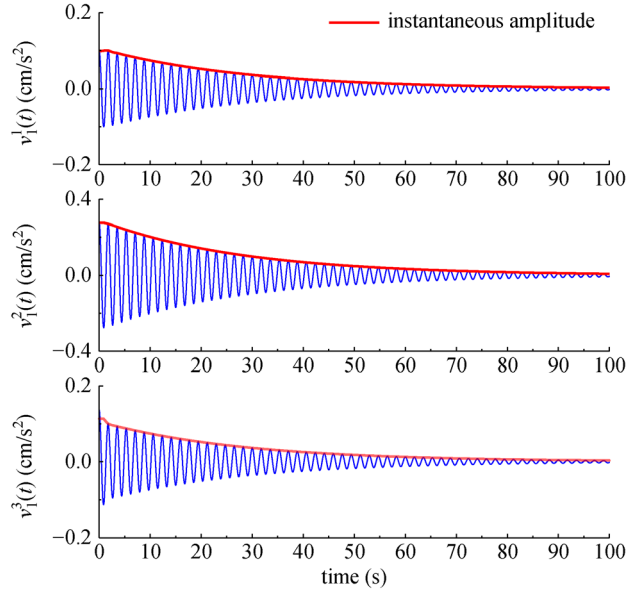

Fig. 6 Modal responses for Mode 1 of a 3-DOF system and instantaneous amplitudes

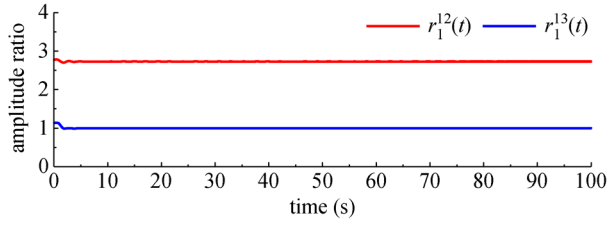

Fig. 7 Amplitude ratios of modal responses for Mode 1

Table 3 Mode shape vectors a 3-DOF system

Mode	Mode shape vector	
	identified	theoretical
1	$[1.00, 2.73, 1.00]^T$	$[1.00, 2.73, 1.00]^T$
2	$[1.00, 0.00, -1.00]^T$	$[1.00, 0.00, -1.00]^T$
3	$[1.00, -0.72, 1.00]^T$	$[1.00, -0.73, 1.00]^T$

ison. It can be seen that the identified results agree very well with the theoretical results. This example demonstrates that the proposed method is capable to identify the modal parameters of systems with closely space modes, which is very commonly seen in civil structures.

3.2 2-DOF system with frequency shift

The second example is a 2-DOF system with FDR $s(t) = v_1(t) + v_2(t)$, as shown in Eq. (15), where $\xi = 0.02$, $f_1 = 0.5$ Hz, $f_2 = 1$ Hz, $f_2' = 0.95$ Hz. The second mode exhibits a sudden frequency shift and amplitude variation at $t = 15$ s, which is used to simulate the occurrence of a sudden damage in the structure. This example is analyzed to demonstrate the ability of the proposed method in capturing a transient frequency change in a signal, which generally reflects a sudden change in structural property during online system monitoring.

$$v_1(t) = \mathrm{e}^{-2\pi\xi f_1 t}\cos(2\pi f_1 t), \tag{15a}$$

$$v_2(t) = \begin{cases} \mathrm{e}^{-2\pi\xi f_2 t}\cos(f_2 t), & 0 < t \leqslant 15 \\ 0.4\mathrm{e}^{-2\pi\xi f_2' t}\cos[f_2'(t-15)], & 15 < t \leqslant 30 \end{cases}. \tag{15b}$$

The FDR (sampling frequency = 100 Hz) and its amplitude spectra are shown in Fig. 8. The amplitude spectra failed to detect the frequency shift due to the limitation of frequency resolution of the Fourier transform. Although the frequency resolution can be increased by increasing the signal length, the Fourier transform cannot capture the exact time instant of the frequency shift.

$s(t)$ is decomposed into two modes using VMD ($K = 2$, as the amplitude spectra in Fig. 8 have two dominant bands), and the results are shown in Fig. 9, in which the exact modal responses (Eq. (15)) are also shown for comparison. It can be seen that the modal responses extracted by VMD agree well with the true ones. EMD is also able to separate the two modes in $s(t)$, while EMD results in several low-energy pseudo-components, as shown in Fig. 10. The instantaneous modal frequencies (denoted as $f_1(t)$ and $f_2(t)$, respectively) of 2 modes are shown in Fig. 11. $f_1(t)$ and $f_2(t)$ agree well with the corresponding true values, and the sudden frequency shift in $v_2(t)$ is successfully captured. The calculated instantaneous modal damping ratios (denoted as $\xi_1(t)$ and $\xi_2(t)$, respectively) shown in Fig. 12 also agree very well with

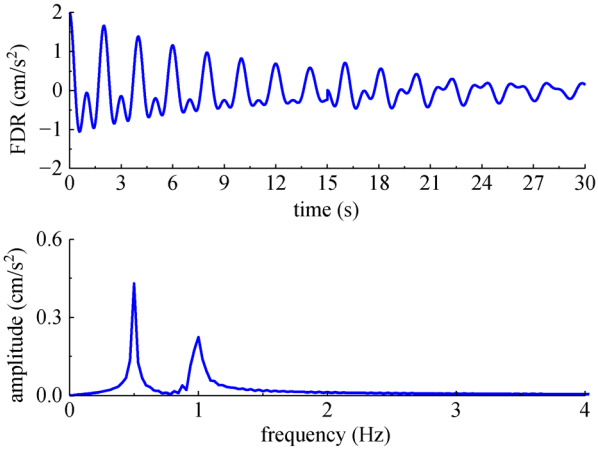

Fig. 8 FDR of a 2-DOF system and amplitude spectra

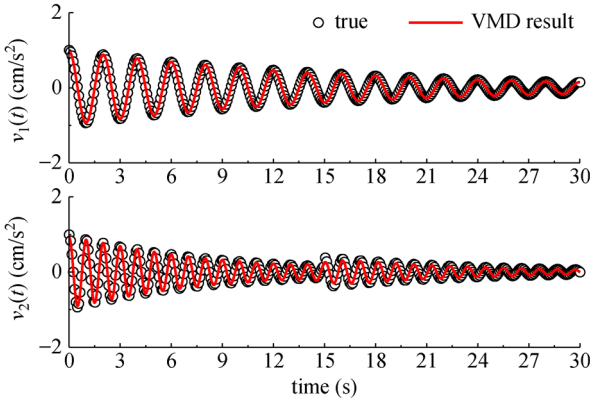

Fig. 9 Modal responses of a 2-DOF system

the true values ($\xi = 0.02$). The remarkable fluctuations of $\xi_1(t)$ and $\xi_2(t)$ around $t = 15$ s are induced by the sudden amplitude variation.

The above example proves that the proposed method is capable to capture a sudden frequency change in a structural vibration signal and the variations of modal parameters. Therefore, the proposed method may serve as an effective tool for detecting the occurrences of sudden damages in online system monitoring of civil structures.

3.3 SDOF nonlinear system: laboratory experimental validation

The third example is a spring-suspended flat plate with 1500 × 600 × 10 (length × width × depth) mm^3 in size and 8.90 kg in mass, as schematically shown in Fig. 13. Such systems have been widely used to study the wind-induced effects on bridge decks [6,47,48], and the specific case in Fig. 13 is designed by Ref. [47] to study the nonlinear air-induced forces on typical bridge decks in wind-off condition. The flat plate (made of wooden plates) is suspended with eight coil springs to simulate the vertical

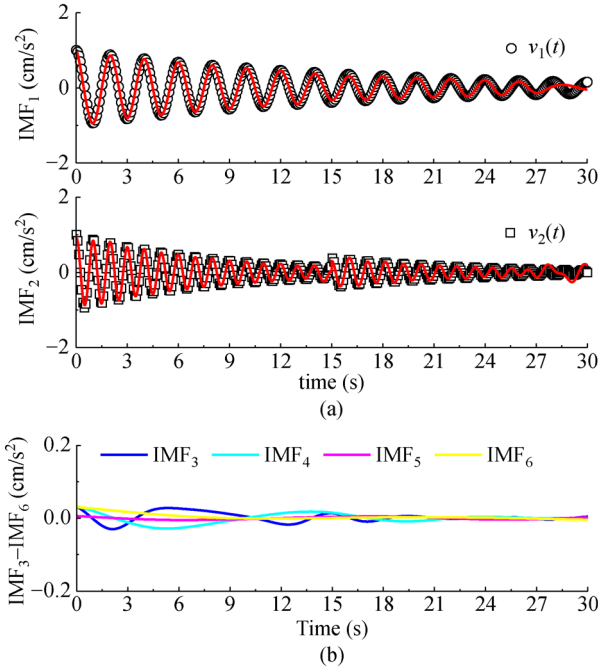

Fig. 10 EMD results for FDR of a 2-DOF system. (a) IMF_1 and IMF_2; (b) $IMF_3 \sim IMF_6$

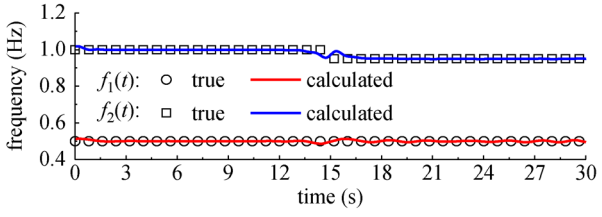

Fig. 11 Modal frequencies of a 2-DOF system

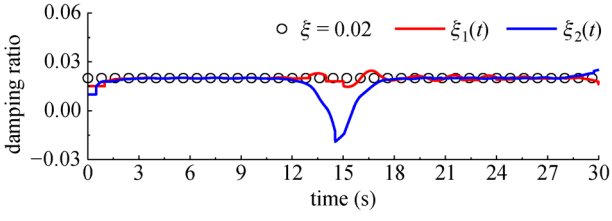

Fig. 12 Modal damping ratios of a 2-DOF system

and torsional modes. The longitudinal distance (LD in Fig. 13) between the springs is 1100 mm, and the transverse distance (TD in Fig. 13) is adjustable to accommodate various torsional frequencies. Three accelerometers (DeltaTraon 4508, Brüel&Kjær, Copenhagen, Denmark) are installed on the flat plate to monitor the vertical accelerations at a sampling frequency of 1024 Hz. The transverse distance between the central axis and the accelerometers is 250 mm. To guarantee two-dimensional flow field [48], two elliptic end plates (major axis = 1200

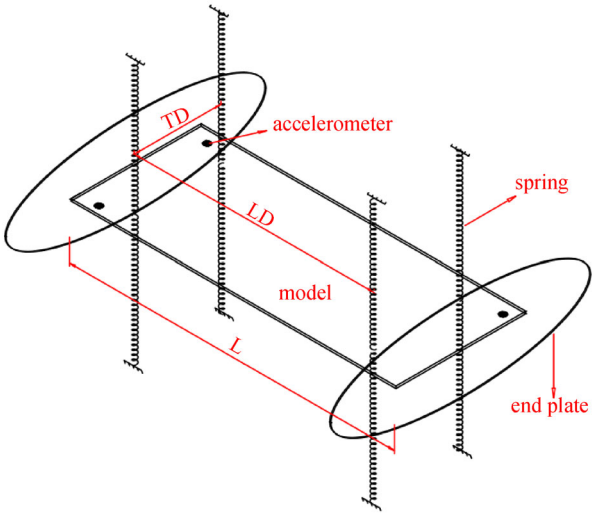

Fig. 13 Schematic diagram of a spring-suspended flat plate system

mm, minor axis = 600 mm, thickness = 4 mm) are attached to both ends of the section models. SDOF (vertical or torsional) free vibration tests were carried out in wind-off conditions to study the nonlinear vibration characteristics of the flat plate, in which the flat plate was excited by releasing from an initial displacement impulse. The time-varying vertical and torsional accelerations of the central axis can be calculated from the signals recorded by the accelerometers. Detailed descriptions of the experimental setup are available in Ref. [47].

One of the recorded FDR and its amplitude spectra is shown in Fig. 14. It can be seen that the FDR contains one dominant frequency band around 1.5 Hz and slight low-frequency components. The low-frequency components may be induced by the zero shifts of the accelerometers, which are commonly encountered by many types of accelerometers [49,50]. Fortunately, it has been demonstrated that VMD is suitable for removing low-frequency and high-frequency noises [34]. The FDR is then decomposed by VMD with $K = 2$. The extracted modal response (denoted as $v(t)$) and its amplitude spectra shown in Fig. 15 indicate that the low-frequency noises are successfully removed. Actually, the low-frequency noises can be removed simply by a high-pass digital filter. However, the phase of the modal response may be affected by the filter, and filters cannot be used to separate closely spaced modes.

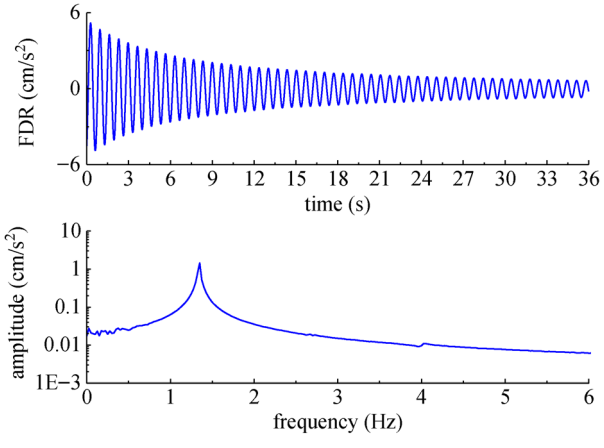

Fig. 14 FDR of a SDOF system and amplitude spectra

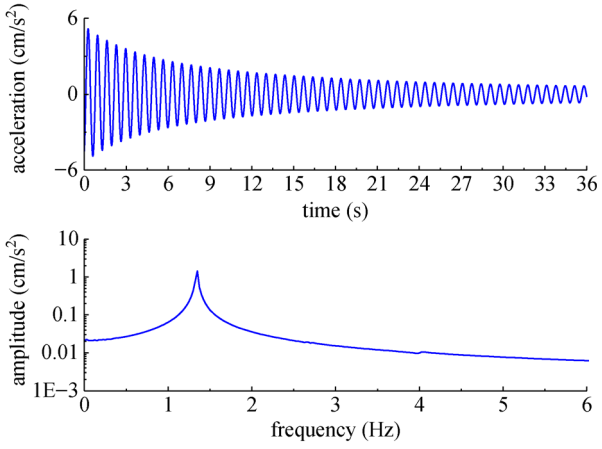

Fig. 15 Modal response of a SDOF system and amplitude spectra

The calculated $f(t)$ and $\xi(t)$ of the modal response are plotted against the vibration amplitude in Figs. 16 and 17, respectively. The observable fluctuations in $f(t)$ and $\xi(t)$ can be ascribed to the slight high-frequency noises, discrete sampling of the recorded signal, and numerical error. $f(t)$ and $\xi(t)$ show clearly features of amplitude-dependence. Therefore, $f(q)$ and $\xi(q)$ are calculated using Eq. (9), as shown in Figs. 16 and 17, respectively.

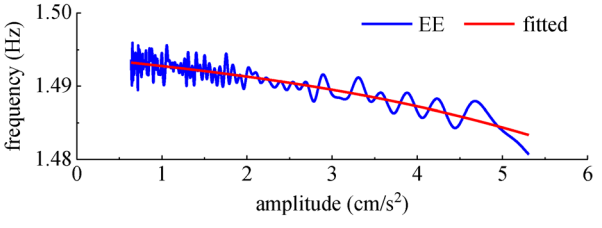

Fig. 16 Modal frequencies of a SDOF system

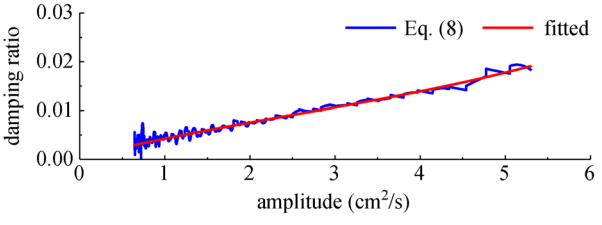

Fig. 17 Modal damping ratios of a SDOF system

To verify the identification accuracies of the modal parameters, $f(q)$ and $\xi(q)$ are substituted into the motion equation [47], and the modal response is calculated step by step using the Newmark-β method from the first sampled peaks. The comparison between the extracted modal response and the calculated one is shown in Fig. 18. The calculated time history agrees very well with the recorded one during the whole length for both amplitudes and phases. Therefore, the accuracies of the identified modal parameters are verified. This example demonstrates that the proposed method can be used for identifying system with amplitude-dependent modal parameters, which is commonly seen in many types of civil structures.

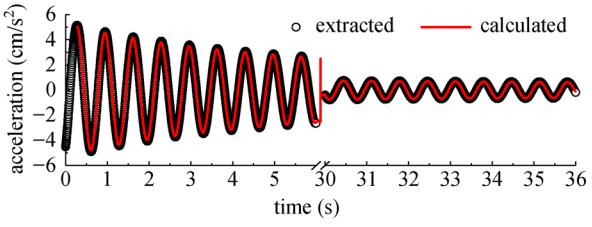

Fig. 18 Comparison between extracted and calculated modal responses

4 Modal parameter identification from ambient vibration response

The preceding section comprehensively demonstrated the capability of the proposed method in identifying modal parameters for different types of systems using free vibration data. However, it is not always possible to conduct free vibration tests especially for large-scale or in-operating structures. Therefore, it is of great interest to show the ability of the proposed method in modal parameter identification using ambient vibration responses. In this section, the proposed method is combined with the widely used RDT [14] to identify the modal parameters of the 3-DOF system in Section 3.1 from ambient vibration responses.

The 3-DOF system is excited by a series of 7200 s long Gaussian white noise (sampling frequency = 100 Hz) with zero mean and 0.2 cm/s^2 standard deviation at the third DOF, and the ambient vibration response of the third DOF is shown in Fig. 19. Such an excitation is definitely unrealistic because a real ambient excitation (wind, traffic, etc.) is by no means fixed at a single point. However, as the main purpose of this section is to show the ability of the proposed method in modal parameter identification from ambient vibration responses, the ambient excitation is predigested to simplify the analysis. The FDR reconstructed from the ambient response in Fig. 19 using RDT is shown in Fig. 20 together with its amplitude spectra. The reconstructed FDR is decomposed into 3 modes (denoted as $v_1(t)$, $v_2(t)$, $v_3(t)$, respectively) by VMD (K = 3) as its

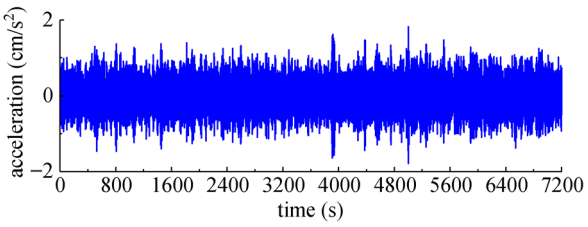

Fig. 19 Ambient vibration response of a 3-DOF system

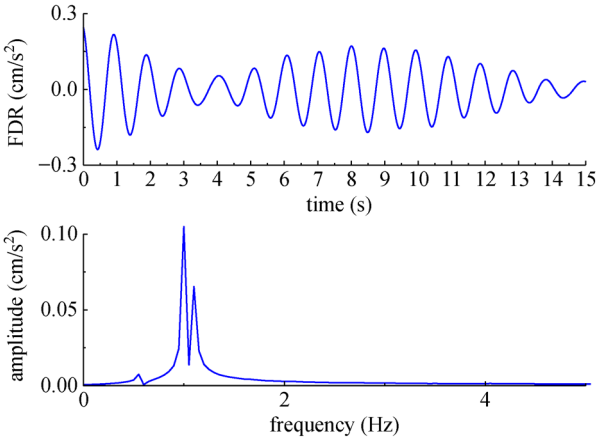

Fig. 20 Reconstructed FDR of a 3-DOF system and its amplitude spectra

amplitude spectra have three dominant bands. The extracted $v_1(t)$, $v_2(t)$, $v_3(t)$ and their instantaneous amplitudes are shown in Fig. 21. The instantaneous modal frequencies (denoted as $f_1(t)$, $f_2(t)$, $f_3(t)$, respectively) and instantaneous modal damping ratios (denoted as $\xi_1(t)$, $\xi_2(t)$, $\xi_3(t)$, respectively) are shown in Figs. 22 and 23, respectively. The instantaneous modal frequencies and instantaneous modal damping ratios agree satisfactorily with the true values. The results for Mode 3 exhibit observable fluctuations, possibly because the energy of Mode 3 in the reconstructed FDR is very low so that the modal response is deteriorated by noises.

The instantaneous modal frequencies and instantaneous modal damping ratios are extracted from the FDRs at all 3 DOFs separately, and the mean values are listed in Table 4. Again, the mean values almost exactly reflect the theoretical values. This example demonstrates that the proposed method can be combined with RDT to identify modal parameters from ambient vibration response.

5 Conclusions

In the present work, an out-put only modal parameter identification method based on VMD is developed for civil structure identifications. VMD is used to decompose the recorded or reconstructed FDR into modal responses. To

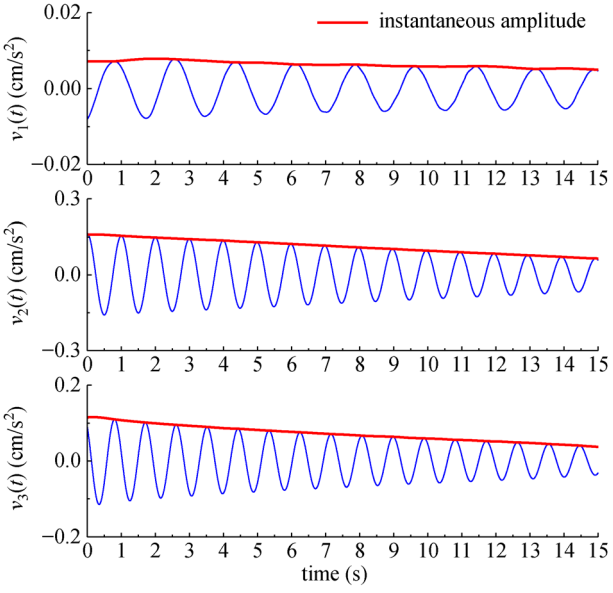

Fig. 21 Modal responses of a 3-DOF system extracted from ambient vibration and instantaneous amplitudes

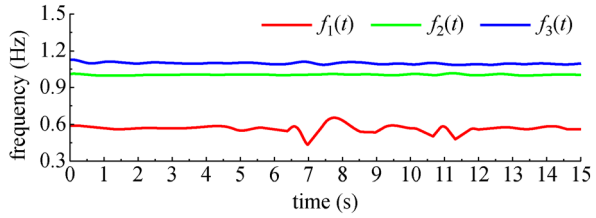

Fig. 22 Modal frequencies of a 3-DOF system extracted from ambient vibration

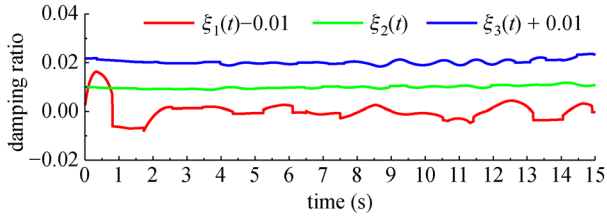

Fig. 23 Modal damping ratios of a 3-DOF system extracted from ambient vibration

Table 4 Mean values of modal frequencies and modal damping ratios of a 3-DOF system extracted from ambient vibrations

Mode	mean[$f(t)$]			mean[$\xi(t)$]		
	1st DOF	2nd DOF	3rd DOF	1st DOF	2nd DOF	3rd DOF
1	0.567	0.567	0.566	0.010	0.010	0.010
2	1.006	unavailable	1.005	0.010	unavailable	0.010
3	1.094	1.093	1.097	0.010	0.010	0.010

capture the possible nonlinear and/or nonstationary features of the modal parameters, the instantaneous modal frequencies are calculated with the EE method, and the instantaneous modal damping ratios are calculated using a newly developed procedure. The proposed method also identifies the mode shape vectors in a straightforward manner by using the modal responses extracted from the FDRs at all available sensors on the structure.

To verify the efficiency and highlight the superiority of the proposed method, several numerical and experimental case studies are analyzed. The superiority of VMD relative to EMD in decomposing certain types of vibration signals is demonstrated. The instantaneous modal frequencies and instantaneous modal damping ratios can detect the existence of nonlinearities and any transient modal parameter variations. The case studies show that the proposed method is efficient and accurate in modal parameter identification for systems with closely spaced modes, sudden modal parameter variation, and amplitude-dependent modal parameters, etc.

Acknowledgements The research is jointly supported by the Fundamental Research Funds for the Central Universities (No. DUT17ZD228), National Program on Key Basic Research Project (973 Program, No. 2015CB057705), and National Natural Science Foundation of China (Grant No. 51478087), which are gratefully acknowledged.

Appendix. Empirical Envelop method

The process of the EE method to calculate the instantaneous amplitude and instantaneous frequency of a mono-component signal $v(t)$ is briefly listed as follows:

1) Perform the AM-FM decomposition [45] to $v(t)$, yields

$$A(t) = q(t), \tag{A1}$$

$$F(t) = \cos[\varphi(t)], \tag{A2}$$

where $A(t)$ is the AM part obtained by cubic spline fitting and an iterative process; $F(t)$ is the FM part.

2) The derivative of $F(t)$ with respect to time can be expressed as

$$F'(t) = -\varphi'(t)\sin[\varphi(t)]. \tag{A3}$$

3) Perform the AM-FM decomposition to $F'(t)$, yields

$$F'(t) = b(t)\cos[\varphi^*(t)] = -b(t)\sin\left[\varphi^*(t) + \frac{\pi}{2}\right]. \quad \text{(A4)}$$

4) It can be seen from Eqs. (A4) and (A5) that $b(t) = \varphi'(t)$. Therefore, the instantaneous frequency of $v(t)$ can be expressed as

$$f(t) = \frac{b(t)}{2\pi}. \quad \text{(A5)}$$

As the EE method obtains the instantaneous frequency of a mono-component signal through two AM-FM decompositions without involving the HT, the limitations of the Bodrosian theorem [43] and Nuttall theorem [44] can be satisfied automatically and the end effects can be greatly reduced [39].

References

1. Nanthakumar S S, Lahmer T, Zhuang X, Zi G, Rabczuk T. Detection of material interfaces using a regularized level set method in piezoelectric structures. Inverse Problems in Science and Engineering, 2016, 24(1): 153–176
2. Nanthakumar S S, Valizadeh N, Park H S, Rabczuk T. Surface effects on shape and topology optimization of nanostructures. Computational Mechanics, 2015, 56(1): 97–112
3. Xia P Q, Brownjohn J M. Bridge structural condition assessment using systematically validated finite-element model. Journal of Bridge Engineering, 2004, 9(5): 418–423
4. Chang K C, Kim C W. Modal-parameter identification and vibration-based damage detection of a damaged steel truss bridge. Engineering Structures, 2016, 122: 156–173
5. Shahdin A, Mezeix L, Bouvet C, Morlier J, Gourinat Y. Monitoring the effects of impact damages on modal parameters in carbon fiber entangled sandwich beams. Engineering Structures, 2009, 31(12): 2833–2841
6. Zhang M J, Xu F Y, Ying X Y. Experimental investigations on the nonlinear torsional flutter of a bridge deck. Journal of Bridge Engineering, 2017, 22(8): 04017048
7. Xue K, Igarashi A, Kachi T. Optimal sensor placement for active control of floor vibration considering spillover effect associated with modal filtering. Engineering Structures, 2018, 165: 198–209
8. Yang S, Allen M S. Output-only modal analysis using continuous-scan laser Doppler vibrometry and application to a 20 kW wind turbine. Mechanical Systems and Signal Processing, 2012, 31: 228–245
9. Bagheri A, Ozbulut O E, Harris D K. Structural system identification based on variational mode decomposition. Journal of Sound and Vibration, 2018, 417: 182–197
10. Bendat J S, Piersol A G. Engineering Applications of Correlation and Spectral Analysis. New York: John Wiley & Sons, 1993
11. Brincker R, Zhang L, Andersen P. Modal identification of output-only systems using frequency domain decomposition. Smart Materials and Structures, 2001, 10(3): 441–445
12. Jacobsen N J, Andersen P, Brincker R. Using enhanced frequency domain decomposition as a robust technique to harmonic excitation in operational modal analysis. In: Proceedings of the International rational Modal Analysis Conference, 2006. Leuven: 2006, 18–20
13. Zhang L, Wang Y, Tamura T. A frequency-spatial domain decomposition (FSDD) method for operational modal analysis. Mechanical Systems and Signal Processing, 2010, 24(5): 1227–1239
14. Ibrahim S R. Random decrement technique for modal identification of structures. Journal of Spacecraft and Rockets, 1977, 14(11): 696–700
15. Juang J N, Pappa R S. An eigensystem realization algorithm for modal parameters identification and model reduction. Journal of Guidance, Control, and Dynamics, 1985, 8(5): 620–627
16. Gautier P E, Gontier C, Smail M. Robustness of an ARMA identification method for modal analysis of mechanical systems in the presence of noise. Journal of Sound and Vibration, 1995, 179(2): 227–242
17. Peeters B, De Roeck G. Stochastic system identification for operational modal analysis: A review. Journal of Dynamic Systems, Measurement, and Control, 2001, 123(4): 659–667
18. Berkooz G, Holmes P, Lumley J L. The proper orthogonal decomposition in the analysis of turbulent flows. Annual Review of Fluid Mechanics, 1993, 25(1): 539–575
19. Vu-Bac N, Lahmer T, Zhuang X, Nguyen-Thoi T, Rabczuk T. A software framework for probabilistic sensitivity analysis for computationally expensive models. Advances in Engineering Software, 2016, 100: 19–31
20. Hamdia K M, Ghasemi H, Zhuang X, Alajlan N, Rabczuk T. Sensitivity and uncertainty analysis for flexoelectric nanostructures. Comput Method Appl Me, 2018, 337: 95–109
21. Hamdia K M, Silani M, Zhuang X, He P, Rabczuk T. Stochastic analysis of the fracture toughness of polymeric nanoparticle composites using polynomial chaos expansions. International Journal of Fracture, 2017, 206(2): 215–227
22. Kijewski T, Kareem A. Wavelet transforms for system identification in civil engineering. Comput-Aided Civ Inf, 2003, 18(5): 339–355
23. Huang N E, Shen Z, Long S R, Wu M C, Shih H H, Zheng Q. The empirical mode decomposition and the Hilbert spectrum for nonlinear and non-stationary time series analysis. Proceedings of the Royal Society of London, Series A, 1998, 454: 903–95
24. Rilling G, Flandrin P, Goncalves P. On empirical mode decomposition and its algorithms. In: IEEE-EURASIP Workshop on Nonlinear Signal and Image Processing, 2003, 8–11
25. Yang J N, Lei Y, Pan S, Huang N. System identification of linear structures based on Hilbert-Huang spectral analysis. Part 1: normal modes. Earthquake Engineering & Structural Dynamics, 2003, 32(9): 1443–1467
26. Yang J N, Lei Y, Pan S, Huang N. System identification of linear structures based on Hilbert-Huang spectral analysis. Part 2: Complex modes. Earthquake Engineering & Structural Dynamics, 2003, 32(10): 1533–1554
27. Chen J, Xu Y L, Zhang R C. Modal parameter identification of Tsing Ma suspension bridge under Typhoon Victor: EMD-HT method. Journal of Wind Engineering and Industrial Aerodynamics, 2004, 92(10): 805–827
28. Pines D, Salvino L. Structural health monitoring using empirical

mode decomposition and the Hilbert phase. Journal of Sound and Vibration, 2006, 294(1–2): 97–124

29. He X H, Hua X G, Chen Z Q, Huang F L. EMD-based random decrement technique for modal parameter identification of an existing railway bridge. Engineering Structures, 2011, 33(4): 1348–1356
30. Shi Z Y, Law S S. Identification of linear time-varying dynamical systems using Hilbert transform and empirical mode decomposition method. Journal of Applied Mechanics, 2007, 74(2): 223–230
31. Bao C, Hao H, Li Z X, Zhu X. Time-varying system identification using a newly improved HHT algorithm. Computers & Structures, 2009, 87(23–24): 1611–1623
32. Peng Z K, Peter W T, Chu F L. An improved Hilbert–Huang transform and its application in vibration signal analysis. J Sound Vib 2005; 23; 286(1–2): 187–205
33. Rilling G, Flandrin P. One or two frequencies? The empirical mode decomposition answers. IEEE Transactions on Signal Processing, 2008, 56(1): 85–95
34. Dragomiretskiy K, Zosso D. Variational mode decomposition. IEEE Transactions on Signal Processing, 2014, 62(3): 531–544
35. Xue Y J, Cao J X, Wang D X, Du H K, Yao Y. Application of the variational mode decomposition for seismic time-frequency analysis. IEEE Journal of Selected Topics in Applied Earth Observations and Remote Sensing, 2016, 9(8): 3821–3831
36. Poornachandran P, Athira S, Harikumar K. Recursive variational mode decomposition algorithm for real time power signal decomposition. Procedia Technology, 2015, 21: 540–546
37. Upadhyay A, Pachori R B. Instantaneous voiced/non-voiced detection in speech signals based on variational mode decomposition. Journal Franklin I, 2015, 352(7): 2679–2707
38. Wang Y, Markert R, Xiang J, Zheng W. Research on variational mode decomposition and its application in detecting rub-impact fault of the rotor system. Mechanical Systems and Signal Processing, 2015, 60–61: 243–251
39. Zheng J D, Cheng J S, Yang Y. A new instantaneous frequency estimation approach-empirical envelope method. Journal of Vibration and Shock, 2012, 31(17): 86–90 (in Chinese)
40. Hestenes M R. Multiplier and gradient methods. Journal of Optimization Theory and Applications, 1969, 4(5): 303–320
41. Liu Y, Yang G, Li M, Yin H. Variational mode decomposition denoising combined the detrended fluctuation analysis. Signal Processing, 2016, 125: 349–364
42. Clough R W, Penzien J. Dynamics of Structures. Berkeley: Computers & Structures Inc, 2003
43. Bedrosian E A. Product theorem for Hilbert transforms. Proceedings of the IEEE, 1963, 51(5): 868–869
44. Nuttall A H, Bedrosian E. On the quadrature approximation to the Hilbert transform of modulated signals. Proceedings of the IEEE, 1966, 54(10): 1458–1459
45. Huang N E, Wu Z H, Long S R, Arnold K C, Chen X Y, Blank K. On instantaneous frequency. Advances in Adaptive Data Analysis, 2009, 1(2): 177–229
46. Siringoringo D M, Fujino Y. System identification of suspension bridge from ambient vibration response. Engineering Structures, 2008, 30(2): 462–477
47. Zhang M J, Xu F Y. Nonlinear vibration characteristics of bridge deck section models in still air. Journal of Bridge Engineering, 2018, 23(9): 04018059
48. Staubli T. Calculation of the vibration of an elastically mounted cylinder using experimental data from forced oscillation. Journal of Fluids Engineering, 1983, 105(2): 225–229
49. Knapp J, Altmann E, Niemann J, Werner K D. Measurement of shock events by means of strain gauges and accelerometers. Measurement, 1998, 24(2): 87–96
50. Acar C, Shkel A M. Experimental evaluation and comparative analysis of commercial variable-capacitance MEMS accelerometers. Journal of Micromechanics and Microengineering, 2003, 13(5): 634–645